

# Journal of Materials Chemistry C

Accepted Manuscript



This is an *Accepted Manuscript*, which has been through the Royal Society of Chemistry peer review process and has been accepted for publication.

*Accepted Manuscripts* are published online shortly after acceptance, before technical editing, formatting and proof reading. Using this free service, authors can make their results available to the community, in citable form, before we publish the edited article. We will replace this *Accepted Manuscript* with the edited and formatted *Advance Article* as soon as it is available.

You can find more information about *Accepted Manuscripts* in the [Information for Authors](#).

Please note that technical editing may introduce minor changes to the text and/or graphics, which may alter content. The journal's standard [Terms & Conditions](#) and the [Ethical guidelines](#) still apply. In no event shall the Royal Society of Chemistry be held responsible for any errors or omissions in this *Accepted Manuscript* or any consequences arising from the use of any information it contains.

# **A promising direct visualization of Au@Ag nanorod-based colorimetric sensor for trace detection of alpha-fetoprotein**

**Fan Zhang, Jian Zhu\*, Jian-Jun Li, Jun-Wu Zhao**

The Key Laboratory of Biomedical Information Engineering of Ministry of Education,

School of Life Science and Technology, Xi'an Jiaotong University,

Xi'an 710049, China

**\* Corresponding author**

**Telephone:** 86-29-82664224

**Fax numbers:** 86-29-82664224

**Email:** zhujian@mail.xjtu.edu.cn

**Address:** School of Life Science and Technology,

Xi'an Jiaotong University,

Xi'an, xian ning west road 28#, 710049,

Peoples Republic of China

**Abstract**

The Ag coating-induced blue shift and enhancement of longitudinal plasmon of Au nanorods result in abundant and tunable optical absorptions in the visible region, which leads to the Au@Ag nanorod becomes a good candidate for colorimetric sensing. In this paper, we have reported an effective and simple approach for visualization detection of alpha-fetoprotein (AFP) based on Au@Ag core-shell nanorods. The AFP concentration-dependent colloid color of Au@Ag core-shell nanorods could change from green to gray, olive to brown, and even blue to violet to pink, which is more abundant color change compared with traditional red to blue color change. Besides, as Ag shell thickness is increased, a dip was observed, which is located between two strong absorption peaks. The change of dip is proposed as a new biosensor parameter for biomolecule detection based on absorption spectrum. AFP concentration detection could be realized according to the change of the position and intensity of the dip, which has not been reported in the biomolecule detection field so far. Au@Ag core-shell nanorods with a small aspect ratio of inner Au nanorods are more suitable for direct readout visualization, with a color change from blue to violet to pink. While from the point of view of spectrum analysis, Au@Ag core-shell nanorods with a great aspect ratio of inner Au nanorods show higher spectral sensitivity. Furthermore, it is found that non-centrifuged Au@Ag core-shell nanorods are preferentially assembled in a side-by-side fashion with the addition of AFP, which will provide new approaches for other kinds of nanorods in controllable assembly fashions.

**Key words:** Au@Ag core-shell nanorods; alpha-fetoprotein (AFP); colorimetric; localized surface plasmon resonance (LSPR)

## 1. Introduction

Nobel metal nanoparticles have attracted great attention in biosensing application due to their unique optical properties. A substantial detection techniques based on nanoparticles including localize surface plasmon resonance (LSPR) induced shift of absorption and scattering,<sup>1</sup> the surface enhanced Raman scattering (SERS),<sup>2</sup> metal-enhanced fluorescence (MEF)<sup>3</sup> as well as fluorescence quenching<sup>4</sup> have been widely studied. Du et al. reviewed the recent development in the design and application of Au nanoparticle-based optical assays for the detection contaminants in forms of colorimetric, light-scattering and fluorescent in detail,<sup>5</sup> of which colorimetric detection induced by LSPR shift exhibits great priority owing to its convenience. The most advantage is that only with the naked eye the detection can be realized. Colorimetric assay based on Au nanoparticles usually involves the color change of 'red to blue' or 'blue to red'.<sup>6</sup> Du et al. summarized Au nanoparticles probes for the colorimetric detection of  $\text{Hg}^{2+}$  based on oligo nucleotides, oligopeptides, and functional molecules in aqueous media.<sup>7</sup> A urine-based plasmonic colorimetric assay of Au nanoparticles was developed by Du et al. to detect  $\text{Hg}^{2+}$  with good selectivity, and a detection limit of 50 nM could be achieved in the real sample.<sup>8</sup>

The Au nanorods have enriched the color change of the Au nanoprobe. Au nanorods have two localized surface plasmon resonance absorption modes, transverse mode and longitudinal mode,<sup>9</sup> which are induced by the oscillation of conduction electrons along two different directions. The longitudinal surface plasmon resonance is sensitive to the aspect ratio (AR) of Au nanorods, which could be tuned easily from visible to near-infrared wavelength region by tailoring their morphologies such as shape and size, as well as local dielectric surrounding environment.<sup>10-14</sup> In the past decades, Au nanorods have been extensively applied in the field of non-aggregation colorimetric-based biosensing. For instance, Au nanorods could be oxidized by a variety of ions including  $\text{NO}_2^-$ ,<sup>15</sup>  $\text{Cu}^{2+}$ <sup>16</sup> as well as  $\text{H}_2\text{O}_2$ ,<sup>17</sup> resulting in shortened length of Au nanorods, and lead to changes in both color and absorption spectra. Based on this mechanism, a series of different colorimetric sensors were designed.<sup>18-19</sup> Besides,

*Revised Manuscript*      *The changes are marked with underline*

---

the targeted molecules induce the aggregation of the nanorods due to interparticle plasmonic coupling, leading to a shift in plasmon absorption peaks, which further enrich the plasmonic response of the nanorods. This change can be easily monitored by means of simple absorption spectrometer, or just directly discerned by naked eye. Xu et al. proposed a label-free detection approach of AFP based on the aggregation of Au nanorods.<sup>20</sup> The addition of  $\text{Cu}^{2+}$  and  $\text{Pb}^{2+}$  could induce the aggregation of the cysteine-modified gold nanorods, which are designed for the detection of  $\text{Cu}^{2+}$  and  $\text{Pb}^{2+}$ .<sup>21-22</sup> The assembly of Au nanorods in the fashion of side-by-side and end-to-end were also applied to the detection of environmental toxin.<sup>23</sup> However, one of the disadvantages of aggregation-based detection is that Au nanorods are unstable and easily coagulated under external environmental changes such as the charge of the colloidal particles,<sup>24</sup> pH value<sup>25-26</sup> and ion strength induced by NaCl.<sup>27</sup> As more and more nanoparticles with tailored morphology are fabricated, silver triangular prisms are also utilized for colorimetric detection. The main mechanism is based on the morphology transition of nanoparticles. In the case of excessive iodine ion, Chen et al. implemented colorimetric detection of mercury ions by using mercury ion for protection of twelve mercaptan-capped Ag nanoprisms morphology changes.<sup>28</sup>

In comparison with colorimetric detection based on aggregation of Au nanorods and morphology transition of Ag nanoparticles, colorimetric sensors designed by generating a shell on surface of the inner core exhibit abundant brilliant color changes. The colorimetric mechanism is that coating shell changes the local dielectric environment of the inner core, leading to the shift of the spectra, thus realizing the target molecule detection.<sup>29-30</sup> For example, Park et al. used Au@Ag core-shell nanocubes to realize the colorimetric detection of sulfur ions with a detection limit of 200 bbp. LSPR shifting covers at a wider band region of 500 to 800 nm, which exhibited the rich color change.<sup>31</sup> Following the same idea, a novel non-aggregation colorimetric sensor for detection of dopamine was developed based on the rapid response of AuNRs– $\text{Ag}^+$  system to dopamine, forming a new structure of Au-Ag core-shell nanorods, which caused the LSPR of AuNRs blue shift accompany with a brilliant color changes of the

colloids.<sup>32</sup> Gao et al. designed a novel Au@Ag nanorods-based probe for the detection of phosphatase activity. This probe could achieve colorimetric detection with high resolution by naked eye. In the presence of phosphatase, ascorbic acid 2 phosphate could be hydrolyzed to ascorbic acid. Ascorbic acid plays a key role in reduction of silver ions to elemental silver, depositing on the surface of the Au nanorods, and leads to a blue shift of surface plasmon resonance absorption peak. The detection is achieved by the color change of Au nanorods colloids from red to orange-yellow-green-blue-purple.<sup>33</sup>

Alpha-fetoprotein (AFP) is one of the biomarker of hepatocellular carcinoma in human serum. The concentration of AFP above the normal level is associated with a series of diseases such as liver cancer.<sup>34</sup> Therefore, the detection of AFP with ultrasensitive is of great help to early clinical diagnosis. Traditional AFP detection including enzyme-linked Immunoassay (ELISA) and radioimmunoassay (RIA) have been widely applied to the clinical and biochemical analysis. However, ELISA suffers from the disadvantage of tedious steps, while RIA usually involves potential health hazards.<sup>35</sup> Ao et al. developed an assay based on the fluorescence quenching of fluorescein isothiocyanate induced by gold nanoparticles coated with monoclonal antibody.<sup>36</sup> Xiang et al. designed a droplet platform for the colorimetric detection of AFP.<sup>37</sup> Hu et al. reported a signal amplification strategy based on surface plasmon resonance imaging chip for the sensitive and specific detection of AFP in human serum.<sup>38</sup> Unfortunately, it often needs to further modification of nanoparticles, and sometimes can be easily affected by the surrounding environment. Although great progress has been made in nanoparticle-based colorimetric ions detection, less is reported when it concerns to the detection of biomarker molecules. As a consequence, developing a simple and rapid colorimetric sensor has significant academic value and application prospect.

Compared with Au nanorods, Ag coated Au nanorods possess unique plasmonic resonance behaviors. The coating of Ag leads to the longitudinal LSPR of Au nanorods blue shift. Four LSPR peaks could be observed, two of which have remarkable intensity and could be fine tuned over the visible region. As we know, color change in

*Revised Manuscript*     *The changes are marked with underline*

---

the visible region offers more advantages for colorimetric detection based on naked eye. Then, could these abundant spectral signals be used for the detection of biomolecules? These fascinating spectral properties and brilliant colors inspire us to design colorimetric biosensor for detection of AFP molecule. Do Au@Ag core-shell nanorods with different aspect ratio of inner Au nanorods exhibit different properties? Accordingly, the following research is to attempt to be engaged in the problems proposed above. In this paper, we develop a trace colorimetric detection of AFP based on Au@Ag core-shell nanorods. The effect of Ag shell thickness and inner Au nanorods aspect ratio on the sensitivity of the AFP detection has also been discussed.

## 2. Experimental Section

### 2.1 Reagents and apparatus

Cetyltrimethyl ammonium bromide (CTAB) was purchased from Sigma-Aldrich. Gold chloride trihydrate ( $\text{HAuCl}_4$ , Sinopharm Chemical Reagent Co. Ltd, Shanghai, China), hydrochloric acid (HCl, Beijing Chemical Works, China) were used as received. Sodium borohydride ( $\text{NaBH}_4$ ), sodium hydroxide (NaOH), silver nitrate ( $\text{AgNO}_3$ ) and ascorbic acid (AA) were obtained from Aladdin. AFP test kits were purchased from Zhengzhou Biocell Biotechnology Co. Ltd. All the reagents were of analytical grade and were used without further purification. The ultrapure water used in all experiments had a resistivity of  $18.2 \text{ M}\Omega\text{cm}^{-1}$

Ultrapure water was obtained from Millipore water purification system (Milli-Q, Millipore, USA). All the absorption spectra were performed on a UV3600 absorption spectrometer (Shimadzu, Japan) with the wavelength range of 300 to 1000 nm. Transmission electron microscopy (TEM) images were obtained from H-600 (Hitachi, Japan) operating at an acceleration voltage of 75 kV. A PB-10 pH meter (Sartorius, Germany) was employed to measure pH values of all the aqueous solutions. Zeta potential of Au@Ag core-shell nanorods was obtained by Zeta Potential Analyzer (Brookhaven, USA).

## 2.2 Preparation of Au@Ag core-shell nanorods with different Ag shell thickness

Au nanorods were prepared by seed-mediated method with slight modification.<sup>39-40</sup> The Au nanorods have a longitudinal plasmon resonance wavelength located at 826 nm, showing a color of pink. Au@Ag core-shell nanorods were synthesized according to the previous approach by using Au nanorod as an inner core.<sup>40-41</sup> By tuning the amount of silver nitrite, Au@Ag core-shell nanorods with various Ag shell thickness could be obtained. Fig. 1a displays the absorption spectra of Au nanorods and Au@Ag core-shell nanorods. Au@Ag core-shell nanorods have two different Ag shell thicknesses. Here, we denote them as Au@Ag 1 with a thin Ag shell and Au@Ag 2 with a thick Ag shell. As we know, Au nanorods have two absorption peaks, corresponding to LSPR modes of longitudinal and transverse respectively. However, Au@Ag core-shell nanorods own four absorption peaks, corresponding to the longitudinal and transverse mode of Au-Ag interface, as well as the longitudinal and transverse mode of the outer Ag shell respectively.<sup>42</sup> Here, we defined as peak 1 to peak 4 from long to short wavelength. When coated with Ag shell on the Au nanorods, peak 1 exhibits a remarkable blue shift accompany with enhanced absorbance intensity. Peak 3 and peak 4 also appeared with increased Ag shell thickness. The colloidal Au@Ag core-shell nanorods with a thin Ag shell exhibits a color of green, and Au@Ag core-shell nanorods with a thick Ag shell exhibits a color of olivine, as can be seen in the inset of Fig. 1a, greatly enriched the color of Au nanorods. At the same time, the plasmonic linewidth of the Au@Ag core-shell nanorods is narrower compared with the original Au nanorods, resulting in the phenomenon knowing as 'plasmonic focusing', which makes it more suitable for biosensor with high quality factor based on spectral analysis.<sup>43</sup> The prepared Au nanorods are stable in aqueous solution with good monodispersity, which exhibit excellent uniformity in dimension according to TEM image, as shown in Fig. 1b. Fig. 1c and Fig. 1d are two typical TEM images of Au@Ag core-shell nanorods with a thin and a thick Ag shell thickness. As demonstrated by TEM images, Au@Ag core-shell nanorods with a thin shell thickness

of about 5.8 nm and Au@Ag core-shell nanorods with a thick shell thickness of about 9.5 nm.

### **2.3 Preparation of Au@Ag core-shell nanorods with different aspect ratios of inner Au nanorod**

Au nanorods with three aspect ratios were prepared by tuning the volume of silver nitrite in growth solution. The obtained Au nanorods have a longitudinal LSPR located at 826 nm, 730 nm and 680 nm respectively. Fig. 2a, Fig. 2b and Fig. 2c are the corresponding TEM images of Au nanorods with great, middle and small aspect ratios. These three different aspect ratios of Au nanorods were denoted as AR 1, AR 2 and AR 3. When coated with Ag, the corresponding Au@Ag core-shell nanorods were denoted as Au@Ag with AR 1, Au@Ag with AR 2 and Au@Ag with AR 3. Fig. 2d is the absorption spectrum of Au@Ag core-shell nanorods with three different aspect ratios of the inner Au nanorod. The dash lines are the absorption spectra of original Au nanorods with three different aspect ratios respectively. Although the Ag shell thickness is roughly the same, due to the different aspect ratio of inner Au nanorods, Au@Ag core-shell nanorods exhibit colors of green, dark green and blue respectively, as depicted in inset of Fig. 2d.

### **2.4 The interaction of Au@Ag core-shell nanorods and AFP with various concentrations of AFP**

Various volumes of 10 ng/mL AFP (0 uL, 6 uL, 8 uL, 10 uL, 12 uL, 14 uL and 16 uL) were added to 1 mL Au@Ag core-shell nanorods colloids, different volume of ultra water were added to ensure the ultimate volume of 2 mL. The ultimate concentrations of the AFP were 0 pg/mL, 30 pg/mL, 40 pg/mL, 50 pg/mL, 60 pg/mL, 70 pg/mL and 80 pg/mL respectively. The incubation was continued for 6 min. The absorption spectra of the mixture were recorded under the same condition described above.

Zeta potential is a proof for the interaction between Au@Ag core-shell nanorods and alpha-fetoprotein. Zeta potential is a measure of effective surface charge of nanoparticles.<sup>44</sup> As is reported by Dougherty, the protein

molecules conjugated with nanoparticles could result in a zeta potential change.<sup>45</sup> The experimentally prepared Au@Ag core-shell nanorods were surrounded by a small amount of positively charged CTAB molecules, and the zeta potential is (41.42±4.53) mV. Upon the addition of the AFP molecules, the zeta potential decreases to (21.85±2.49) mV. We learn from the literature that alpha-fetoprotein (AFP) is an oncofetal glycoprotein with a molecule weight of 65-kDa and isoelectric point of AFP is 4.7, so in the solution of pH value above 4.7, AFP exhibits negatively charged characteristic.<sup>46</sup> In our experiment, AFP molecules are absorbed on the surface of Au@Ag core-shell nanorods due to electrostatic adsorption, thus reducing the surface potential of the nanorods slightly.

### **3. Results and Discussion**

#### **3.1 The effect of Ag shell thickness on absorption spectra of Au@Ag core-shell nanorods upon the addition of AFP**

The coated Ag shell endows Au nanorods more excellent optical properties. It takes some time for the AFP to interact with Au@Ag core-shell nanorods. Therefore, the effect of the interaction time between the Au@Ag core-shell nanorods and AFP was studied at first. The absorption spectra of Au@Ag core-shell nanorods upon the addition of AFP were recorded by fiber optical spectrometer with an increment of 0.5 min for 10 min. As shown in Fig. 3a, with the increase of interaction time, the absorbance intensity decreased accompany with the blue shift of peak 1, and remained unchanged when the interaction time was more than 10 min, showing that the interaction between Au@Ag core-shell nanorods and AFP was completed within 10 min. The inset of Fig. 3a shows that the distinct change could be observed within 6 min and after that the variation slowed. Thus, the incubation time of 6 min was adopted in the subsequent work.

In order to investigate the effect of Ag shell thickness on Au@Ag core-shell nanorods upon the addition of

*Revised Manuscript*      *The changes are marked with underline*

---

AFP, we compared the absorption spectra of both Au nanorods and Au@Ag core-shell nanorods upon the addition of different concentration of AFP ranging from 0 to 80 pg/mL. Au@Ag core-shell nanorods have two different Ag shell thicknesses corresponding to a thin Ag shell thickness and a thick Ag shell thickness. Here, we chose the Au nanorods whose longitudinal LSPR is located at 826 nm as samples. Utilizing this Au nanorod as a core, we obtained Au@Ag core-shell nanorods with two different Ag shell thicknesses via adjusting the amount of silver nitrate, which were denoted as Au@Ag 1 with a thin Ag shell thickness and Au@Ag 2 with a thick Ag shell thickness.

Fig. 3b displays the absorption spectra of the interaction between AFP and Au nanorods, and the AFP concentrations are ranging from 0 to 80 pg/mL. The introduction of AFP only induces the slight absorbance decrease of the Au nanorods' longitudinal LSPR, while it has little effect on peak position of the Au nanorods. The corresponding color change of Au nanorods upon the addition of AFP is shown in the inset of Fig. 3b. It is obvious that color change was not discerned just by naked eye.

When a thin Ag shell is coated on the Au nanorods, a direct color change was observed to the solution of the interaction between AFP and Au nanorods. Fig. 3c displays the absorption spectra of the interaction between AFP and Au@Ag core-shell nanorods, of which Au@Ag core-shell nanorods have a thin Ag shell thickness corresponding to Au@Ag 1, and the AFP concentrations are ranging from 0 to 80 pg/mL. As is clearly observed in Fig. 3c, as AFP concentration is increased gradually, the wavelength of peak 1 blues shift, accompanying a gradually reduced absorbance; At the same time, the wavelength of peak 2 shows a red shift and enhanced absorbance. It is both the changes of peak position and absorbance intensity of Au@Ag 1 that leads to the color changes in inset of Fig. 3c. Here, the blue shift and the decreased intensity of peak 1 contribute greatly to the color change. The detection system produces a color change from bright green to light violet in response to an increase of AFP concentration. It is found that the Au@Ag core-shell nanorods with a thin Ag shell thickness could realize the

*Revised Manuscript*      *The changes are marked with underline*

---

trace colorimetric detection of AFP, with a detection limit of as low as 30 pg/mL. And what is needed is only one absorption spectrometer after the incubation of just six minutes. The approach is convenient and quick, and do not need complicated instrument.

We continue to increase the Ag shell thickness of the Au@Ag core-shell nanorods, and then obtain a thick Ag shell thickness corresponding to the Au@Ag 2. Compared with Au@Ag 1, the absorbance of peak 1 and peak 2 reach the same intensity. Fig. 3d displays the absorption spectra of the interaction between AFP and Au@Ag 2, and the AFP concentrations are ranging from 0 to 80 pg/mL. The addition of AFP has little effect on the peak position and absorbance intensity of Au@Ag 2. The color changes from olivine to brownish yellow, as shown in the inset of Fig. 3d. However, what attracts us most is the change of the dip, which is located between peak 1 and peak 2. As the AFP concentration is increased, the wavelength of the dip is slightly red shifted and the absorbance intensity is gradually increased at the same time. When the concentration of AFP is 80 pg/mL, the original two peaks denoted as peak 1 and peak 2 are merged into one, and the dip between peak 1 and peak 2 disappears and transforms into a wide peak ultimately.

We have noticed that of all the biomolecular detection based on nanoparticles absorption spectra analyses, the mainly used parameters are peak wavelength and absorbance intensity of LSPR. However, LSPR absorption spectrum changes induced by noble metal nanostructures with different morphologies and ingredients are far more than them. There are more abundant spectral signals, such as the dip between two peaks, linewidth, the division and integration of the adjacent peaks and the relative intensity change of different peaks. For example, Becker et al. found that coating Ag shell on the surface of the Au nanorods lead to the narrowing of plasmonic linewidth, knowing as 'plasmonic focusing'. It helps to enhance the figure of merit of the sensors, thus improving the overall performance of the sensors.<sup>43</sup> However, little attention has been paid on them and let alone the utilization of them. Therefore, it is quite necessary for people to explore the deeper information underlying the normal spectral lines

*Revised Manuscript*     *The changes are marked with underline*

---

and search for new sensor parameters, which is of extraordinary significance for improving sensor sensitivity. As demonstrated in Fig. 3d, the position and intensity of the dip are AFP concentration-dependent. It provides us with a new sensor parameter-'dip', which is located between two strong absorption peaks position. AFP concentration detection could be realized according to the change of the position and intensity of the dip, which has been not reported in the biological molecules detection field so far.

### **3.2 Optimization of the Au@Ag core-shell nanorods with proper aspect ratio of inner Au nanorods for the direct visualization of colorimetric detection of AFP**

In the previous section, inner Au nanorods of Au@Ag core-shell nanorods have a LSPR absorption peak located at 826 nm, which is corresponding to a great aspect ratio. Here we denote it as Au@Ag with AR 1. When Au@Ag with AR 1 have an interaction with different concentrations of AFP, the color changes from light green to dark green then to light purple, which is not discernable for readout visualization, as shown in Fig. 3c. In order to further optimize the Au@Ag core-shell nanorods with proper aspect ratio of inner Au nanorods for the direct visualization of colorimetric detection of AFP, we change inner Au nanorods with different aspect ratios while maintaining the Ag shell thickness the same.

We choose Au nanorods whose longitudinal LSPR absorption peak is 730 nm as samples. When coated with Ag, we denote samples as Au@Ag with AR 2, whose Ag shell thickness is the same with Au@Ag with AR 1. Fig. 4a displays the absorption spectra of the interaction between AFP and Au@Ag with AR 2, and the AFP concentrations are ranging from 0 to 80 pg/mL. As AFP concentration is increased gradually, the wavelength of peak 1 blues shift gradually, accompanying a reduced absorbance, at the same time, the wavelength of peak 2 shows a red shift and enhanced absorbance. The changing trends of both peak 1 and peak 2 are the same as Au@Ag with AR 1, and the color changes from green to blackish green then to violet, as shown in inset of Fig. 4a. The color

change is more easily perceived with naked eye compared with the color change of Au@Ag with AR 1.

For colorimetric detection, the target-induced spectral shifts lead to the visually detectable color change is in the first priority. It is well known that the most sensitive region of the color perception for naked eye of human is preferentially in the region of 500 to 600 nm.<sup>30</sup> Therefore, we continue to reduce the aspect ratio of inner Au nanorods, making the longitudinal LSPR absorption peak located at 680 nm. Similarly, when coated with Ag, we denote samples as Au@Ag with AR 3, whose Ag shell thickness is the same with Au@Ag with AR 1. The peak 1 of Au@Ag with AR 3 is located at 600 nm. Fig. 4b displays the absorption spectra of the interaction between AFP and Au@Ag with AR 2, and the AFP concentrations are ranging from 0 to 80 pg/mL. In terms of Au@Ag with AR 3, similar changing trends in both peak 1 and peak 2 are observed compared with Au@Ag with AR1 and Au@Ag with AR 2. What attracts us most is the corresponding vigorous color change, which achieves a transition from blue green - blue - purple - light purple - pink. This color range is more suitable for naked eye to distinguish the color change, compared with the other two groups of Au@Ag core-shell nanorods. Therefore, from the point of view of macroscopic colorimetric, Au@Ag with AR 3, which is Au@Ag with a small aspect of inner Au nanorods, is more suitable for direct readout visualization.

When Au@Ag core-shell nanorods have an interaction with different concentrations of AFP, different aspect ratios of inner Au nanorods perform different changes on peak 1. In order to investigate the effect of aspect ratio of inner Au nanorods on the peak 1, we draw the comparison of the AFP concentration-dependent the absorbance peak wavelength change of LSPR, as shown in Fig. 4c. Over the AFP concentration range of 0 to 80 pg/mL, the peak 1 of Au@Ag with AR 1 has a 56 nm wavelength shift while it is only 20 nm for Au@Ag with AR 2 and Au@Ag with AR 3. From the point of view of absorption spectrum, Au@Ag core-shell nanorods with a great aspect ratio of inner Au nanorods show higher spectral sensitivity.

### 3.3 The colorimetric sensing mechanism of AFP based on Au@Ag core-shell nanorods

In our experiment, the sensing of AFP is achieved by assembly of Au@Ag core-shell nanorods upon the addition of AFP. The prepared Au@Ag core-shell nanorods were surrounded by a small amount of positively charged CTAB molecules. AFP is negatively charged in the solution of pH value above its isoelectric point. Therefore, AFP molecules are absorbed on the surface of Au@Ag core-shell nanorods due to electrostatic adsorption. The prepared Au@Ag core-shell nanorods have a uniform size distribution with good dispersity, as shown in Fig. 5a. Upon the addition of AFP molecules, Au@Ag core-shell nanorods are assembled in a fashion of side-by-side due to electrostatic absorption, as illustrated in Fig. 5b. The CTAB on the lateral side is more than the end, which lead to the AFP molecules absorbed on the lateral side more than that of the end, thus causing the side-by-side assembly of Au@Ag core-shell nanorods, which results in the distinct changes of the absorption spectrum. According to the absorption spectra, the decreased intensity and blue shift of the peak 1 induced by side-by-side assembly of Au@Ag core-shell nanorods could be observed. The change of the absorption spectra leads to the color change of the Au@Ag core-shell nanorods colloids, thus the colorimetric detection could be realized.

### 3.4 AFP molecules induce aggregation of non-centrifuged and centrifuged Au@Ag core-shell nanorods

All Au@Ag core-shell nanorods samples used above are not treated through centrifugation, surrounding by a small amount of surfactant CTAB. After three days, the color is still unchanged. We choose Au@Ag core-shell nanorods the same as section 3.1, with the inner Au nanorods longitudinal LSPR located at 826 nm. The only difference between previously Au@Ag 1 and the currently Au@Ag core-shell nanorods is that former is directly prepared, the latter is centrifuged at a speed of 10000 rpm for 20 min. However, when we use centrifuged Au@Ag core-shell nanorods to interact with different concentrations of AFP ranging from 0 to 80 pg/mL, the absorption

*Revised Manuscript      The changes are marked with underline*

---

spectrum shows little changes. Then we continue to increase AFP concentration range, 0-550 pg/mL. Fig. 6a shows the absorption spectra of centrifuged Au@Ag core-shell nanorods interact with different concentration of AFP, and the inset is the corresponding color change. The color changes from green to cyan to gray to transparent.

In order to understand the effect of AFP concentration on Au@Ag core-shell nanorods resonance absorption peak more clearly, we plot the AFP concentration-dependent change of peak 1. As can be seen in Fig. 6b, as the concentration of AFP is increased from 0 to 400 pg/mL, the wavelength of peak 1 red shifts slightly. When the concentration of AFP is over 400 pg/mL, drastic red shift could be observed. The intensity of absorbance is decreased at all the AFP concentration range of 0 to 550 pg/mL. For the comparison of centrifuged Au@Ag core-shell nanorods and non-centrifuged Au@Ag core-shell nanorods, similarly, we plot the AFP concentration-dependent change of peak 1 of non-centrifuged Au@Ag core-shell nanorods, whose absorption spectra were shown in Fig. 3c. As is depicted in Fig. 6c, the wavelength of peak 1 blue shifts accompany with the decrease of absorbance intensity. When AFP molecules are introduced into the colloidal of centrifuged Au@Ag core-shell nanorods and non-centrifuged Au@Ag core-shell nanorods respectively, different absorption spectra could be observed. It is observed red shift of peak 1 for centrifuged Au@Ag core-shell nanorods as the AFP concentration increased while blue shift for non-centrifuged Au@Ag core-shell nanorods. Both of them exhibit a decrease in absorbance intensity. Two strikingly different color changes could be observed. For non-centrifuged Au@Ag core-shell nanorods, when interacted with different concentrations of AFP ranging from 0 to 80 pg/mL, its color change from green to violet to light violet, as shown in inset of Fig. 3c. While in terms of centrifuged Au@Ag core-shell nanorods, when the AFP concentration is 50 pg/mL, little color change is observed. As the AFP concentration is increased from 50pg/mL to 550 pg/mL, the color changes from green to cyan to gray to transparent, as shown in inset of Fig. 6c.

The TEM images of non-centrifuged and centrifuged Au@Ag core-shell nanorods colloids upon the addition

*Revised Manuscript*     *The changes are marked with underline*

---

of AFP are compared in Fig. 5b and Fig. 6d. In the case of non-centrifuged Au@Ag core-shell nanorods, an obvious side-by-side assembly of Au@Ag core-shell nanorods can be observed, while there is no obvious side-by-side assembly in the case of centrifuged Au@Ag core-shell nanorods. Therefore, the decreased absorbance intensity and blue shift of LSPR wavelength is attributed to the side-by-side assembly of Au@Ag core-shell nanorods, which is similar to the results of literatures.<sup>23, 47-48</sup> However, it is necessary to note that the shift of LSPR wavelength also depends on the refractive index of surrounding environment. The increased refractive index of surrounding environment often lead to the red shift of the absorption peak,<sup>49</sup> but this effect is much weaker than the side-by-side assembly of Au@Ag core-shell nanorods. Hence, we deduce that the blue shift of absorption peak is induced by the side-by-side assembly of Au@Ag core-shell nanorods. In comparison, there is no obvious side-by-side assembly in the case of centrifuged Au@Ag core-shell nanorods. The addition of AFP with a higher concentration will increase the refractive index of surrounding environment, thus it is the increase of refractive index of surrounding environment that plays a major role in the red shift of absorption peak of Au@Ag core-shell nanorods.

### **3.5 The effect of pH on absorption spectra of Au@Ag core-shell nanorods upon the addition of AFP**

The effect of pH on the absorbance intensity of the analytical system was also investigated in the detection of AFP. Phosphate buffer saline (PBS), which is usually served as a preferable media of nanoparticle for biosensing, is selected in this study.<sup>50-51</sup> Here, we chose Au@Ag with AR 3 which were mentioned in the section 3.2 as samples. The absorbance intensity of peak 1 of Au@Ag core-shell nanorods decreased significantly at pH value of 6 with the addition of 30 pg/mL AFP, as shown in Fig. 7a. The prepared Au@Ag core-shell nanorods colloid exhibits a color of blue, while in the PBS solution of pH value of 6, it turned to green color. The introduction of AFP makes the color of Au@Ag core-shell nanorods change violet in just a few seconds, as demonstrated in the inset of Fig. 7a. Similar changes could be observed when the pH value of the PBS solution changes to 8.8, as shown in Fig. 7b. In

pH value of 6 and 8.8, colorimetric sensing could also be observed. A concentration of 30 pg/mL AFP could lead to a distinct decrease in absorbance intensity and blue shift, which shows greater sensitivity compared with a solution of pH 7. However, according to the research of Orendorff, too acidic or alkaline solution, such as solutions of pH values below 4 or above 9, makes the nanorods easy to aggregate uncontrollably, which will have an impact on the detection of AFP.<sup>44</sup> Therefore, it is recommended for the test system in a proper pH range. By comparing the color change of the Au@Ag core-shell nanorods colloids upon the addition of AFP, one can find that the test media of ultrawater is more suitable for colorimetric detection of AFP by naked eye.

### **3.6 The selectivity for colorimetric detection of AFP based on Au@Ag core-shell nanorods**

As we know, selectivity plays a significant role in estimating the performance of a new biosensor. Therefore, some potential existing biomolecules including bovine serum albumin (BSA), cysteine (Cys), histidine (His) and glycine (Gly) were tested to evaluate the selectivity of the assay with the determination of AFP in this study. We chose Au@Ag with AR 3 which were mentioned in the section 3.2 as samples. The results are summarized in Fig. 8. Here, the concentration of AFP is 80 pg/mL, while the concentration of BSA, Cys, His and Gly was three orders of magnitude higher than that of AFP. As shown in the inset of Fig. 8, the absorbance intensity of Au@Ag core-shell nanorods has a distinct decrease accompany with a blue shift upon the addition of AFP, while there is very little change for BSA, Cys, His and Gly. Meanwhile, distinct color change from blue to violet could be observed due the presence of AFP and the other molecules make the colors stay unchanged, as can be seen in the inset of Fig. 8. Even in such a relatively higher concentration, the potential interfere biomolecules have little effect on the absorbance intensity and resonance wavelength shift of Au@Ag core-shell nanorods, which indicates that this assay have a good selectivity. However, the electrostatic absorption between the positively charged Au@Ag core-shell nanorods and negatively charged AFP cannot guarantee the sensing selectivity compared with antigen-antibody

*Revised Manuscript*      *The changes are marked with underline*

---

recognition. There are other molecules that also could cause the same absorption spectra change of the Au@Ag core-shell nanorods. For example, the addition of glucose could result in the aggregation of Au nanorods in assembly, thus inducing the color change of the colloids.<sup>52</sup> Thus, the shortcoming of this detecting strategy is that it is direct and without further modification of Au@Ag core-shell nanorods, which may be easily unstable when faced with the complex environment such as real patients' serum. However, blood plasma in human is more complex, there are many factors that will influence the optical properties of Au@Ag core-shell nanorods. For example, some other molecules may have the same influence of the absorption spectra, thus affecting the detection of targeted molecules. Therefore, considering the complicated system of human serum, it still has a long way to go for the detection of AFP in the patients' serum. We think this study will provide a basis of research for the further study of the application of nanoparticles in real samples especially for colorimetric detection in the near future.

#### 4. Conclusions

In summary, we have developed an effective and simple approach for visualization detection of AFP based on Au@Ag core-shell nanorods with a detection limit of as low as 30 pg/mL. The color changes blue green to purple to pink, more suitable for naked eye to discern, making it a good candidate for the colorimetric trace detection of AFP. Besides, a new biosensor parameter-'dip' was proposed for biomolecule detection based on absorption spectra due to the increased Ag shell thickness. AFP concentration detection could be realized according to the change of the position and intensity of the dip, which has been not reported in the biomolecule detection field so far. It is of extraordinary significance for exploring the deeper information hidden behind the normal spectral signals and further improving sensor sensitivity. Au@Ag core-shell nanorods with a small aspect ratio of inner Au nanorods is more suitable for direct readout visualization, while from the point of view of spectrum analysis, Au@Ag core-shell nanorods with a great aspect ratio of inner Au nanorods show higher spectral sensitivity. Furthermore, it is found

*Revised Manuscript      The changes are marked with underline*

---

that non-centrifuged Au@Ag core-shell nanorods are preferentially assembled in a side-by-side fashion with the addition of AFP, which will provide new approaches for other kinds of nanorods in controllable assembly fashions. These results will have great potential in developing nanoparticle-based colorimetric sensor for trace detection of biomolecules.

#### **Acknowledgement**

We acknowledge the financial supports of the Fundamental Research Funds for the Central Universities under grant No. 2011jdgz17 and the National Natural Science Foundation of China under grant No. 11174232, 61178075 and 81101122.

**References**

- [1] X. Liu, Q. Dai, L. Austin, J. Coutts, G. Knowles, J.H. Zou, H. Chen and Q. Huo, *J. Am. Chem. Soc.*, 2008, **130**, 2780
- [2] C.D. Chen, S.F. Cheng, L.K. Chau and C.C. Wang, *Biosens. Bioelectron.*, 2007, **22**, 926
- [3] A.M. Gabudean, M. Focsan and S. Astilean, *J. Phys. Chem. C*, 2012, **116**, 12240
- [4] L.G. Xu, H. Kuang, L.B. Wang and C.L. Xu, *J. Mater. Chem.*, 2011, **21**, 16759
- [5] J.J. Du, B.W. Zhu, X.J. Peng and X.D. Chen, *Small*, 2014, **10**, 3461
- [6] T.T. Lou, Z.P. Chen, Y.Q. Wang and L.X. Chen, *ACS Appl. Mater. Inter.*, 2011, **3**, 1568
- [7] J.J. Du, L. Jiang, Q. Shao, X.G. Liu, R.S. Marks, J. Ma and X.D. Chen, *Small*, 2013, **9**, 1467
- [8] J.J. Du, B.W. Zhu and X.D. Chen, *Small*, 2013, **9**, 4104
- [9] C.J. Murphy, T.K. Sau, A.M. Gole, C.J. Orendorff, J.X. Gao, L.F. Gou, S.E. Huayadi and T. Li, *J. Phys. Chem. B*, 2005, **109**, 13857
- [10] S. Link and M.A. El-Sayed, *Annu. Rev. Phys. Chem.*, 2003, **54**, 331
- [11] C. Noguez, *J. Phys. Chem. C*, 2007, **111**, 3806
- [12] K.S. Lee and M.A. El-Sayed, *J. Phys. Chem. B*, 2006, **110**, 19220
- [13] X.H. Huang, S. Neretina and M.A. El-Sayed, *Adv. Mater.*, 2009, **21**, 4880
- [14] Y.G. Sun and Y.N. Xia, *Analyst*, 2003, **128**, 686
- [15] Z.P. Chen, Z.Y. Zhang, C.L. Qu, D.W. Pan and L.X. Chen, *Analyst*, 2012, **137**, 5197
- [16] T. Wen, H. Zhang, X.P. Tang, W.G. Chu, W.Q. Liu, Y.L. Ji, Z.J. Hu, S. hou, X.N. Hu and X.C. Wu, *J. Phys. Chem. C*, 2013, **117**, 25769
- [17] G. Chandrasekar, K. Mouglin, H. Haidara, L. Vidal and E. Gnecco, *Appl. Surf. Sci.*, 2011, **257**, 4175
- [18] Z.Y. Zhang, Z.P. Chen, D.W. Pan and L.X. Chen, *Langmuir*, 2015, **31**, 643

*Revised Manuscript*     *The changes are marked with underline*

---

- [19] J.M. Liu, X.X. Wang, L. Jiao, M.L. Cui, L.P. Lin, L.H. Zhang and S.L. Jiang, *Talanta*, 2013, **116**, 199
- [20] X. Xu, Y.B. Ying and Y.B. Li, *Sensor: Actuat. B-Chem.*, 2012, **175**, 194
- [21] J.M. Liu, H.F. Wang and X.P. Yan, *Analyst*, 2011, **136**, 3904
- [22] H.H. Cai, D.W. Lin, J.H. Wang, P.H. Yang and J.Y. Cai, *Sensor: Actuat. B-Chem.*, 2014, **196**, 252
- [23] L.B. Wang, Y.Y. Zhu, L.G. Xu, W. Chen, H. Kuang, L.Q. Liu, A. Agarwal, C.L. Xu and N.A. Kotov, *Angew. Chem. Int. Edit.*, 2010, **49**, 5472
- [24] T.E. Pylaev, V.A. Khanadeev, B.N. Khlebtsov, L.A. Dykmana, V.A. Bogatyrev and N.G. Khlebtsov, *Colloid J.*, 2011, **73**, 368
- [25] J. Nam, N.Y. Won, H. Jin, H.Y. Chung and S.J. Kim, *J. Am. Chem. Soc.*, 2009, **131**, 13639
- [26] B.Y. Chu, T.T. Qi, J.F. Liao, J.R. Peng, W.T. Li, S.Z. Fu, F. Luo and Z.Y. Qian, *Sensor: Actuat. B-Chem.*, 2012, **166**, 56
- [27] J. Bhamore, K.A. Rawat, H.K. Basu, R.K. Singhal and K. Kailasa, *Sensor: Actuat. B-Chem.*, 2015, **212**, 526
- [28] L. Chen, X.L. Fu, W.H. Lu and L.X. Chen, *ACS Appl. Mater. Interfaces*, 2012, **5**, 284
- [29] H. Huang, Q. Li, J.H. Wang, Z. Li, X.F. Yu and P.K. Chu, *Plasmonics*, 2014, **9**, 11
- [30] J.R. Hao, B. Xiong, X.D. Cheng, Y. He and E.S. Yeung, *Anal. Chem.*, 2014, **86**, 4663
- [31] G. Park, C.Y. Lee, D.H. Seo and H.J. Song, *Langmuir*, 2012, **28**, 9003
- [32] J.M. Liu, X.X. Wang, M.L. Cui, L.P. Lin, S.L. Jiang, L. Jiao and L.H. Zhang, *Sens. Actuators B-Chem.*, 2013, **176**, 97
- [33] Z.Q. Gao, K.C. Deng, X.D. Wang, M. Miro and D.P. Tang, *ACS Appl. Mater. Interfaces*, 2014, **6**, 18243
- [34] Y.J. Teramura and H. Iwata, *Anal. Biochem.*, 2007, **365**, 201
- [35] Y. F. Chang, R.C. Chen, Y.J. Lee, S.C. Chao, L.C. Su, Y.C. Li and C. Chou, *Biosens. Bioelectron.*, 2009, **24**, 1610

*Revised Manuscript*     *The changes are marked with underline*

---

- [36] L.M. Ao, F. Gao, B.F. Pan, R. He and D.X. Cui, *Anal. Chem.*, 2006, **78**, 1104
- [37] X. Xiang, L. Chen, C.L. Zhang, M. Luo, X.H. Ji and Z.K. He, *Analyst*, 2012, **137**, 5586
- [38] W.H. Hu, H.M. Chen, Z.Z. Shi and L. Yu, *Anal. Biochem.*, 2014, **453**, 16
- [39] T.K. Sau and C.J. Murphy, *Langmuir*, 2004, **20**, 6414
- [40] J. Zhu, F. Zhang, J.J. Li and J.W. Zhao, *Sensor. Actuat. B-Chem.*, 2013, **183**, 556
- [41] R.B. Jiang, H.J. Chen, L. Shao, Q. Li and J.F. Wang, *Adv. Mater.*, 2012, **24**, OP200
- [42] J. Zhu, F. Zhang, J.J. Li and J.W. Zhao, *Gold Bull.*, 2014, **47**, 47
- [43] J. Becker, I. Zins, A. Jakab, Y. Khalavka, O. Schubert and C. Sonnichsen, *Nano lett.*, 2008, **8**, 1719
- [44] C.J. Orendorff, P.L. Hankins and C.J. Murphy, *Langmuir*, 2005, **21**, 2022
- [45] G.M. Dougherty, K.A. Rose, J.B.H. Tok, S.S. Pannu, F.Y. S. Chuang, M. Y. Sha, G. Chakarova and S.G. Penn, *Electrophoresis*, 2008, **29**, 1131
- [46] M. Irony-Tur-Sinai, N. Grigoriadis, A. Lourbopoulos, F. Pinto-Maaravi and T. Brenner, *Exp. Neurol.*, 2006, **198**, 136
- [47] H.S. Park, A. Agarwal, N.A. kotov and O.D. Lavrentovich, *Langmuir*, 2008, **24**, 13833
- [48] L.B. Zhong, X. Zhou, S.X. Bao, Y.F. Shi, Y. Wang, S.M. Hong, Y.C. Huang, X. Wang, Z.X. Xie and Q.Q. Zhang, *J. Mater. Chem.*, 2011, **21**, 14448
- [49] K.M. Mayer and J.H. Hafner, *Chem. Rev.*, 2011, **111**, 3828
- [50] C. G. Wang and J. Irudayaraj, *Small*, 2008, **4**, 2204
- [51] C. X. Yu and J. Irudayaraj, *Anal. Chem.*, 2007, **79**, 572
- [52] X.L. Ren, L.Q. Yang, J. Ren and F.Q. Tang, *Nanoscale Res. Lett.*, 2010, **5**, 1658

**List of Fig. captions:**

**Fig. 1:** (a) The absorption spectra of Au@Ag nanorods with different Ag shell thickness, the inset: The corresponding color of Au nanorods and Au@Ag nanorods with a thin and a thick Ag shell thickness; (b) The typical TEM image of Au nanorods, the longitudinal LSPR of Au nanorods is 826 nm; The typical TEM image of Au@Ag nanorods (c) with a thin Ag shell thickness; (d) with a thick Ag shell thickness.

**Fig. 2:** The typical TEM images of Au nanorods (a) with a great aspect ratio, the longitudinal LSPR of Au nanorods is 826 nm; (b) with a middle aspect ratio, the longitudinal LSPR of Au nanorods is 730 nm; (c) with a small aspect ratio, the longitudinal LSPR of Au nanorods is 680 nm; (d) The absorption spectra of Au@Ag core-shell nanorods with three different aspect ratios of the inner Au nanorod, the inset: The corresponding color of Au@Ag nanorods with three different aspect ratios of the inner Au nanorod.

**Fig. 3:** (a) The absorption spectra of Au@Ag nanorods upon the addition of AFP with an increment of 0.5 min for 10 min, the inset: The change of peak wavelength and absorbance intensity with time increased; (b) The absorption spectra of the interaction between AFP and Au nanorods, and the AFP concentrations are ranging from 0 to 80 pg/mL, the inset: The corresponding color change of Au nanorods upon the addition of AFP with different concentrations ranging from 0 to 80 pg/mL; (c) The absorption spectra of the interaction between AFP and Au@Ag core-shell nanorods, of which the Ag shell has a thin thickness (Au@Ag 1), and the AFP concentrations are ranging from 0 to 80 pg/mL, the inset: The corresponding color change of Au@Ag 1 upon the addition of AFP with different concentrations ranging from 0 to 80 pg/mL; (d) The absorption spectra of the interaction between AFP and Au@Ag core-shell nanorods, of which the Ag shell has a thick thickness (Au@Ag 2), and the AFP concentrations are ranging from 0 to 80 pg/mL, the inset: The corresponding color change of Au@Ag 2 upon the addition of AFP

with different concentrations ranging from 0 to 80 pg/mL.

**Fig. 4:** (a) The absorption spectra of the interaction between AFP and Au@Ag nanorods, of which the inner Au nanorods have a middle aspect ratio (AR 2), and the AFP concentrations are ranging from 0 to 80 pg/mL, the inset: The corresponding color change of AR 2 upon the addition of AFP with different concentrations ranging from 0 to 80 pg/mL; (b) The absorption spectra of the interaction between AFP and Au@Ag nanorods, of which the inner Au nanorods have a small aspect ratio (AR 3), and the AFP concentrations are ranging from 0 to 80 pg/mL, the inset: The corresponding color change of AR 3 upon the addition of AFP with different concentrations ranging from 0 to 80 pg/mL; (c) The comparison of AFP concentration-dependent peak wavelength change of Au@Ag nanorods with three different aspect ratios.

**Fig. 5:** TEM images of non-centrifuged Au@Ag nanorods (a) in the absence of AFP; (b) in the presence of AFP.

**Fig. 6:** (a) The absorption spectra of the interaction between centrifuged Au@Ag nanorods and AFP, and the AFP concentration ranges from 0 to 550 pg/mL, the inset: The corresponding color change of centrifuged Au@Ag nanorods upon the addition of AFP with different concentrations ranging from 0 to 550 pg/mL; The AFP concentration-dependent peak wavelength and absorbance change of (b) centrifuged Au@Ag nanorods; (c) non-centrifuged Au@Ag nanorods; (d) TEM image of centrifuged Au@Ag nanorods upon the addition of AFP.

**Fig. 7:** (a) The absorption spectra change of prepared original Au@Ag nanorods, Au@Ag nanorods in PBS of pH 6 in the absence and presence of AFP, the inset: the corresponding color change of prepared Au@Ag nanorods

*Revised Manuscript      The changes are marked with underline*

---

colloids; (b) The absorption spectra change of prepared original Au@Ag nanorods, Au@Ag nanorods in PBS of pH 8.8 in the absence and presence of AFP, the inset: the corresponding color change of prepared Au@Ag nanorods colloids.

**Fig. 8:** The absorption spectra of Au@Ag nanorods upon the addition of different kinds of biomolecules including AFP, BSA, Cys, His and Gly. The concentration of AFP is 30 pg/mL, while the concentration of other biomolecules is 30 ng/mL, the inset 1: The corresponding color of Au@Ag nanorods upon the addition of AFP, BSA, Cys, His and Gly, the inset 2: The absorbance intensity change of Au@Ag nanorods upon the addition of AFP, BSA, Cys, His and Gly.

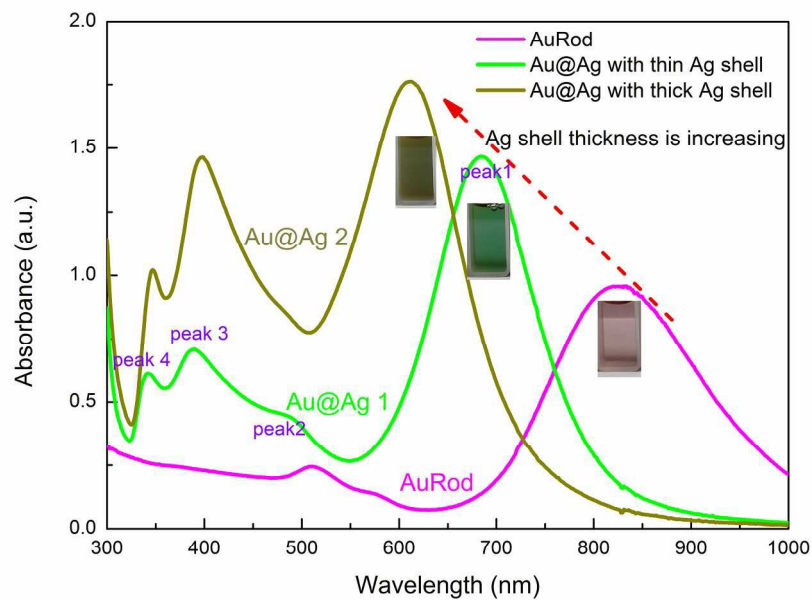


Figure 1a : The absorption spectra of Au@Ag nanorods with different Ag shell thickness, the inset: The corresponding color of Au nanorods and Au@Ag nanorods with a thin and a thick Ag shell thickness; 209x148mm (300 x 300 DPI)

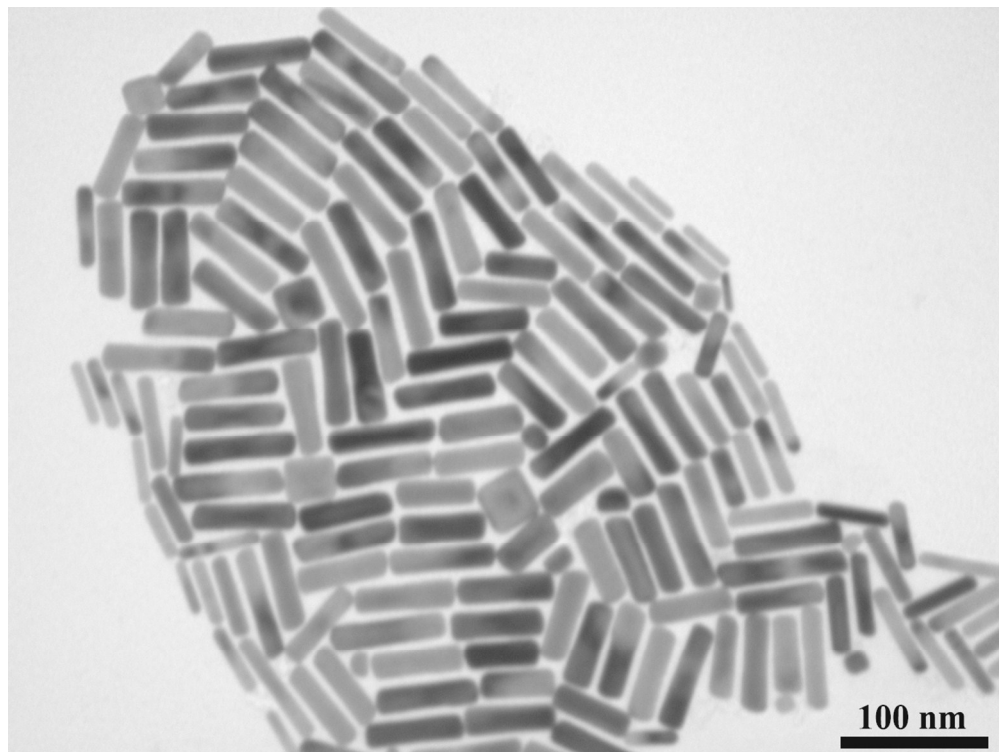


Figure 1b : The typical TEM image of Au nanorods, the longitudinal LSPR of Au nanorods is 826 nm;  
485x363mm (72 x 72 DPI)

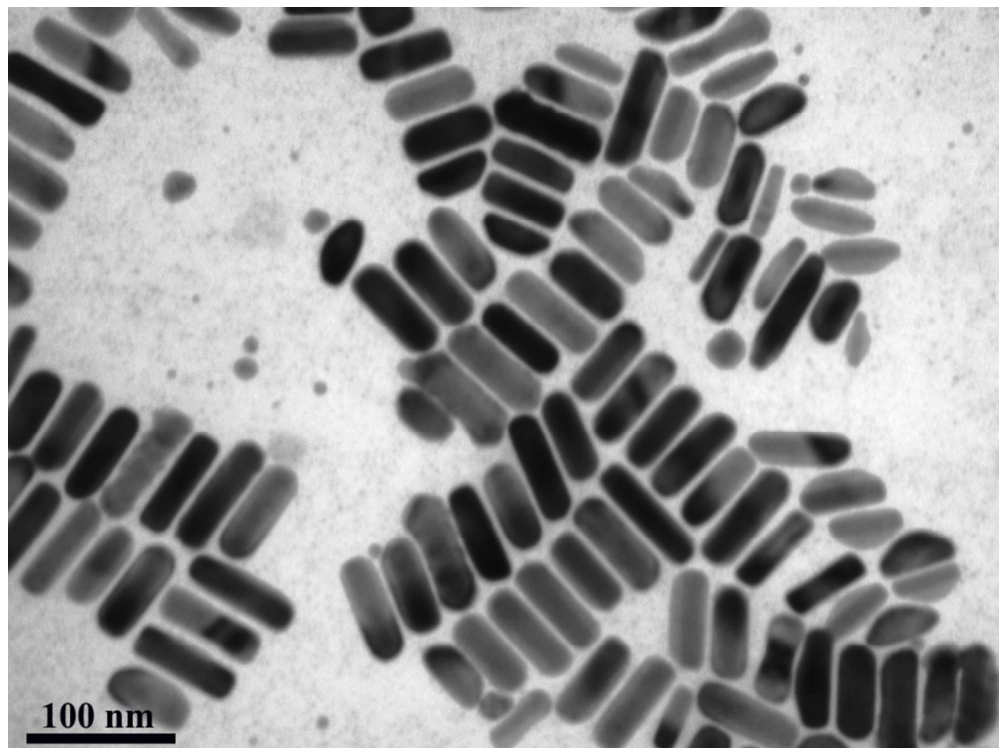


Figure 1c : The typical TEM image of Au@Ag nanorods with a thin Ag shell thickness;  
130x96mm (200 x 200 DPI)

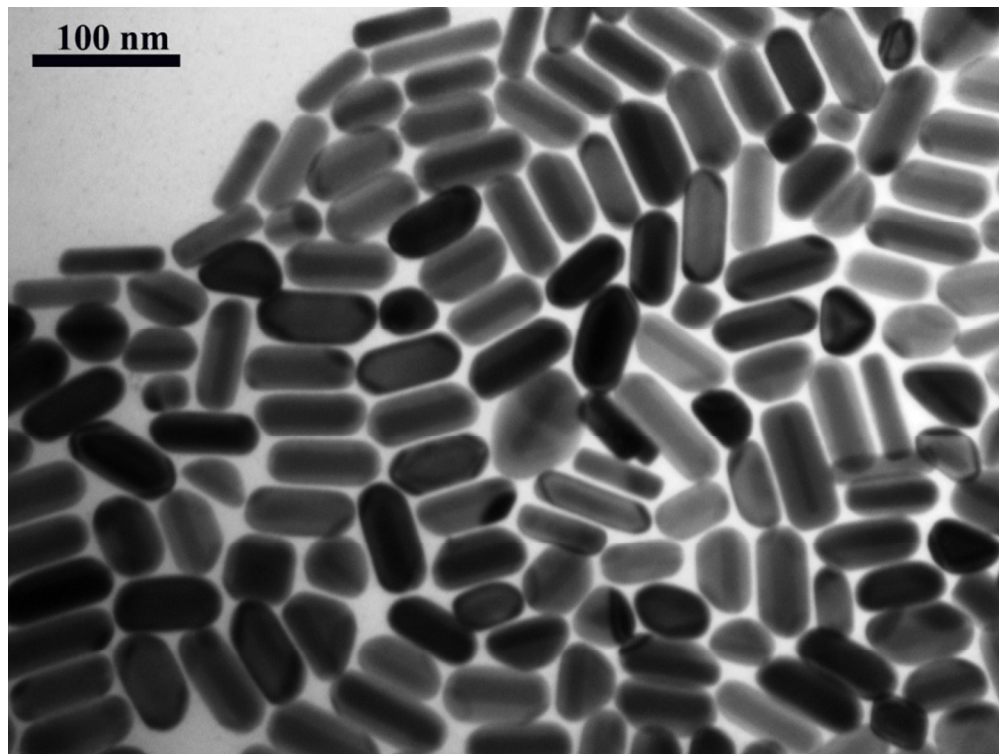


Figure 1d: The typical TEM image of Au@Ag nanorods with a thick Ag shell thickness.  
130x97mm (200 x 200 DPI)

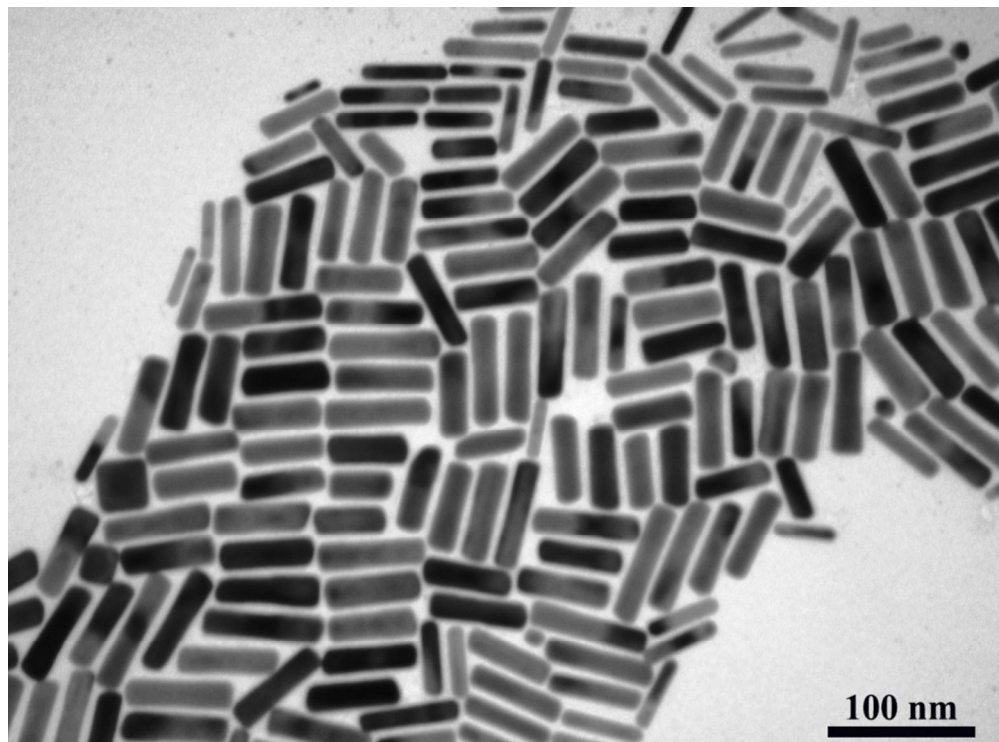


Figure 2a: The typical TEM image of Au nanorods with a great aspect ratio, the longitudinal LSPR of Au nanorods is 826 nm;  
130x96mm (200 x 200 DPI)

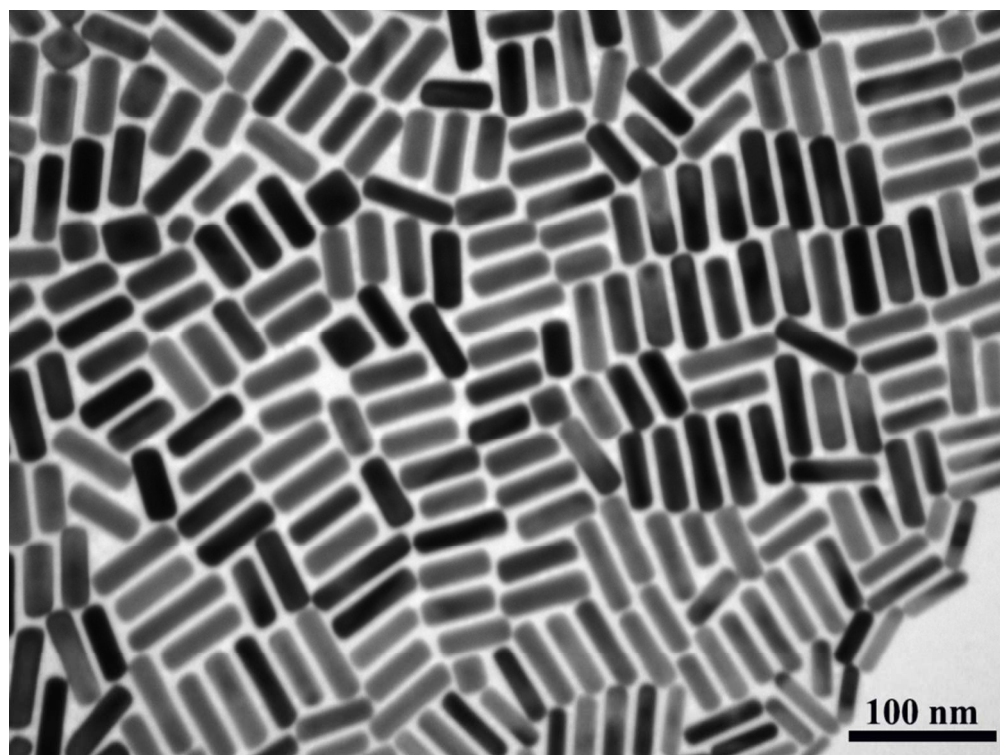


Figure 2b: The typical TEM image of Au nanorods with a middle aspect ratio, the longitudinal LSPR of Au nanorods is 730 nm;  
130x97mm (200 x 200 DPI)

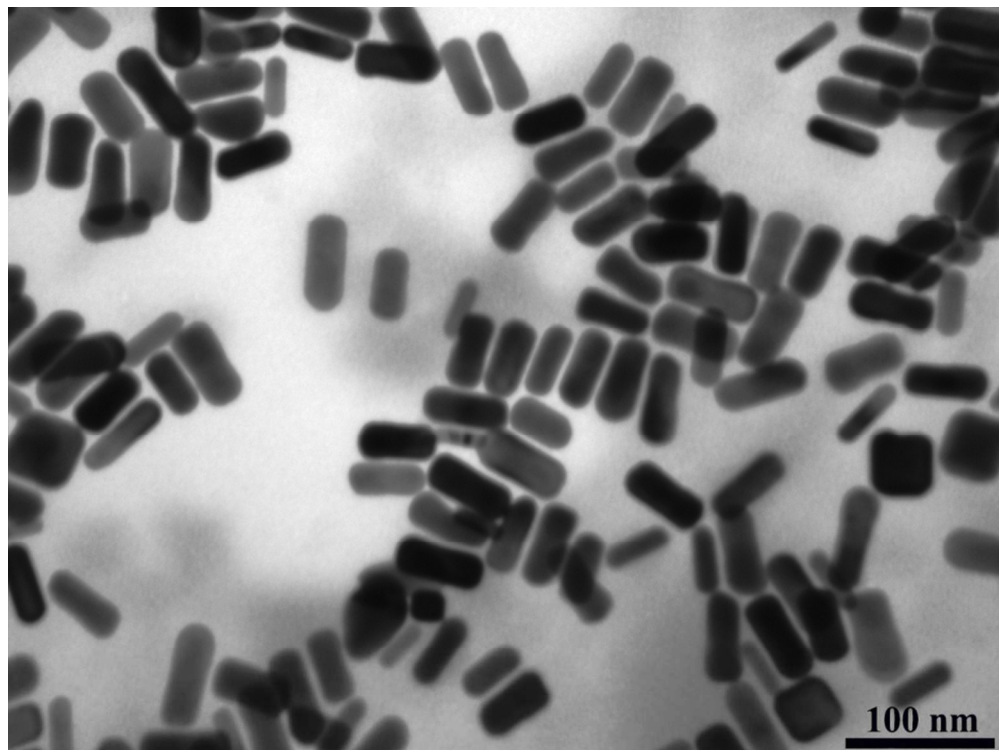


Figure 2c: The typical TEM image of Au nanorods with a small aspect ratio, the longitudinal LSPR of Au nanorods is 680 nm;  
130x97mm (200 x 200 DPI)

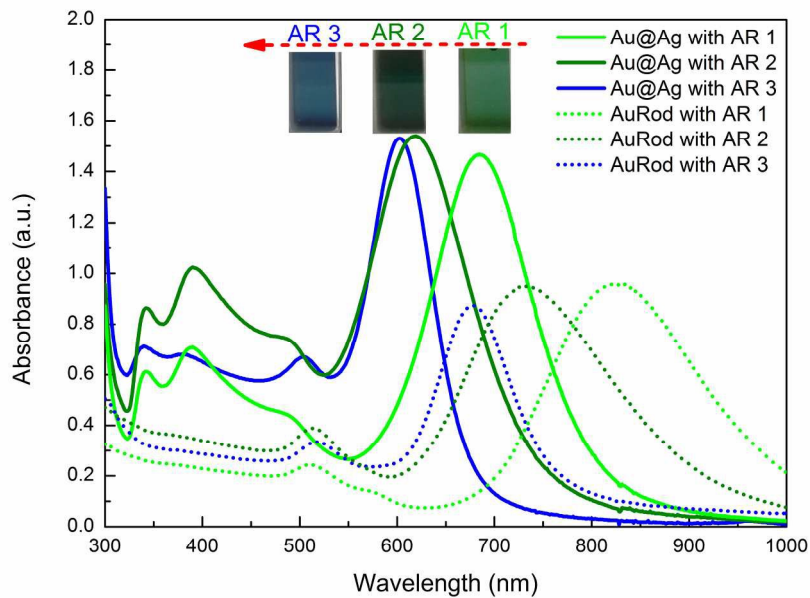


Figure 2d: The absorption spectra of Au@Ag core-shell nanorods with three different aspect ratios of the inner Au nanorod, the inset: The corresponding color of Au@Ag nanorods with three different aspect ratios of the inner Au nanorod.  
209x148mm (300 x 300 DPI)

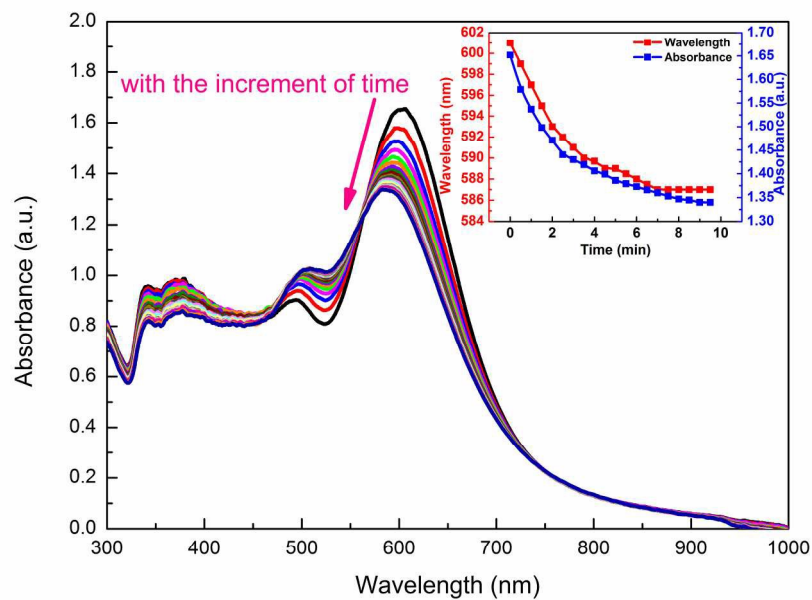


Figure 3a: The absorption spectra of Au@Ag nanorods upon the addition of AFP with an increment of 0.5 min for 10 min, the inset: The change of peak wavelength and absorbance intensity with time increased; 209x148mm (300 x 300 DPI)

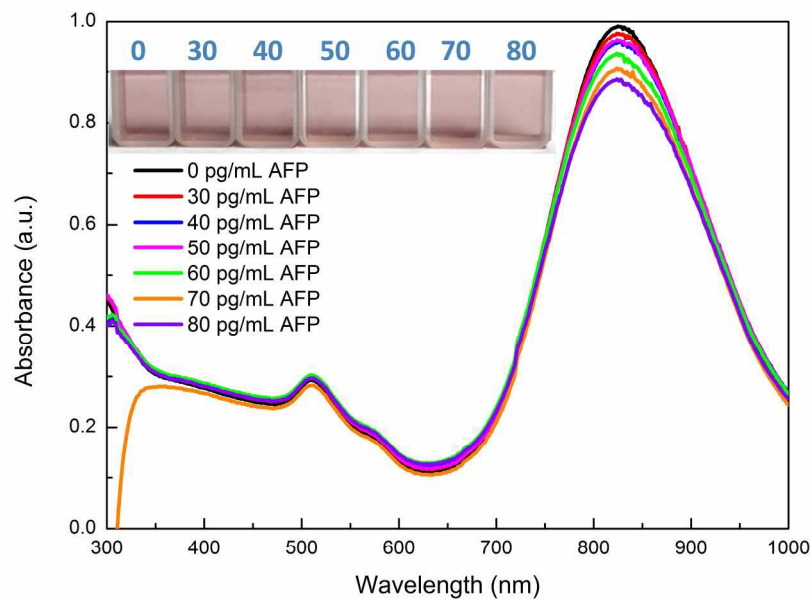


Figure 3b: The absorption spectra of the interaction between AFP and Au nanorods, and the AFP concentrations are ranging from 0 to 80 pg/mL, the inset: The corresponding color change of Au nanorods upon the addition of AFP with different concentrations ranging from 0 to 80 pg/mL; 209x148mm (300 x 300 DPI)

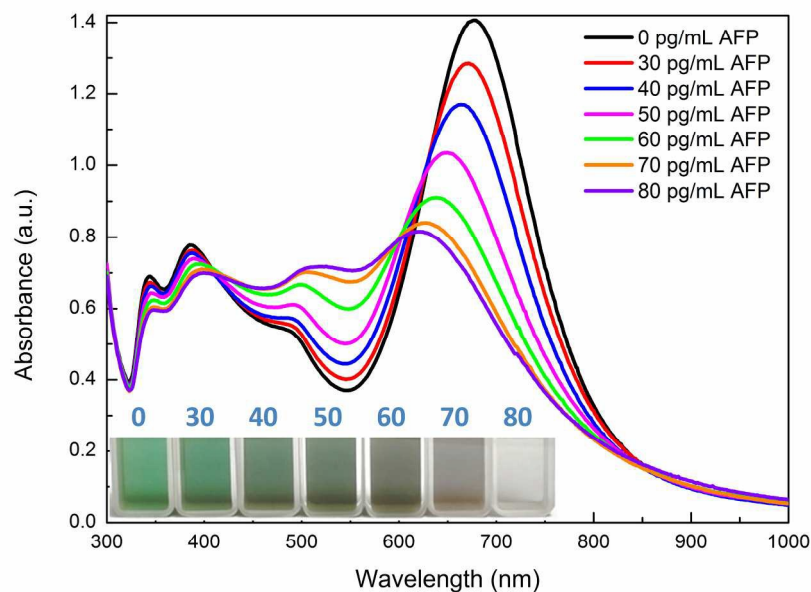


Figure 3c: The absorption spectra of the interaction between AFP and Au@Ag core-shell nanorods, of which the Ag shell has a thin thickness (Au@Ag 1), and the AFP concentrations are ranging from 0 to 80 pg/mL, the inset: The corresponding color change of Au@Ag 1 upon the addition of AFP with different concentrations ranging from 0 to 80 pg/mL; 209x148mm (300 x 300 DPI)

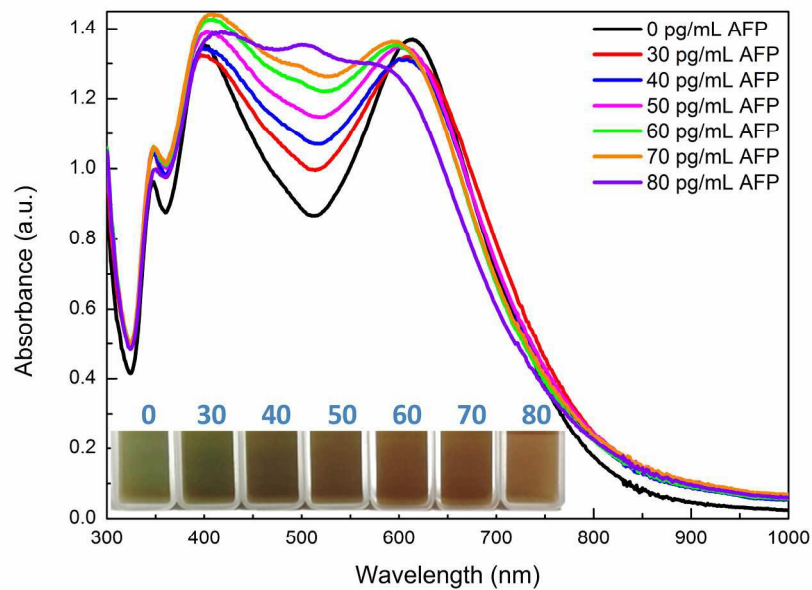


Figure 3d: The absorption spectra of the interaction between AFP and Au@Ag core-shell nanorods, of which the Ag shell has a thick thickness (Au@Ag 2), and the AFP concentrations are ranging from 0 to 80 pg/mL, the inset: The corresponding color change of Au@Ag 2 upon the addition of AFP with different concentrations ranging from 0 to 80 pg/mL.  
209x148mm (300 x 300 DPI)

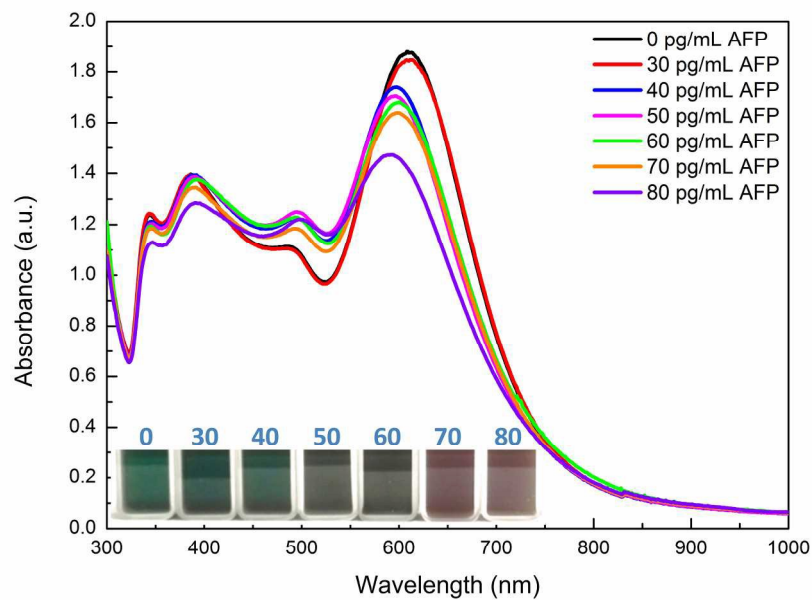


Figure 4a: The absorption spectra of the interaction between AFP and Au@Ag nanorods, of which the inner Au nanorods have a middle aspect ratio (AR 2), and the AFP concentrations are ranging from 0 to 80 pg/mL, the inset: The corresponding color change of AR 2 upon the addition of AFP with different concentrations ranging from 0 to 80 pg/mL; 209x148mm (300 x 300 DPI)

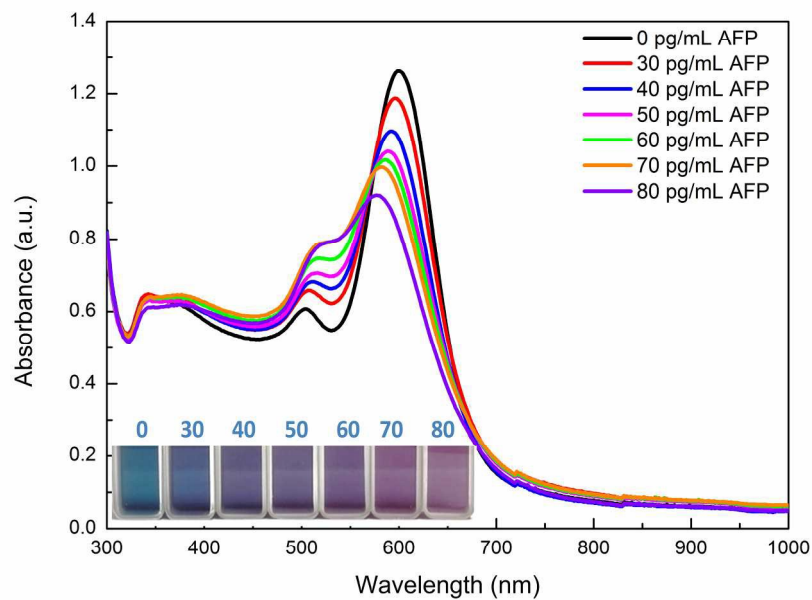


Figure 4b: The absorption spectra of the interaction between AFP and Au@Ag nanorods, of which the inner Au nanorods have a small aspect ratio (AR 3), and the AFP concentrations are ranging from 0 to 80 pg/mL, the inset: The corresponding color change of AR 3 upon the addition of AFP with different concentrations ranging from 0 to 80 pg/mL; 209x148mm (300 x 300 DPI)

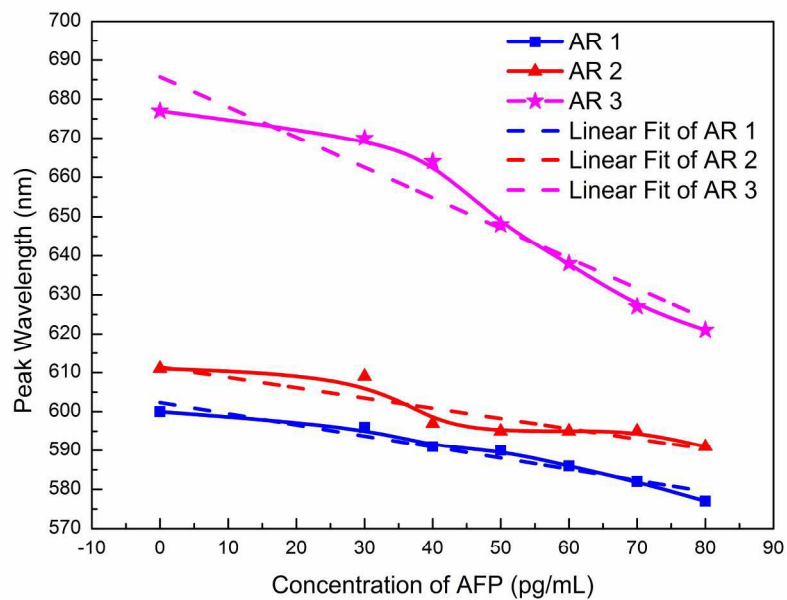


Figure 4c: The comparison of AFP concentration-dependent peak wavelength change of Au@Ag nanorods with three different aspect ratios.  
209x148mm (300 x 300 DPI)

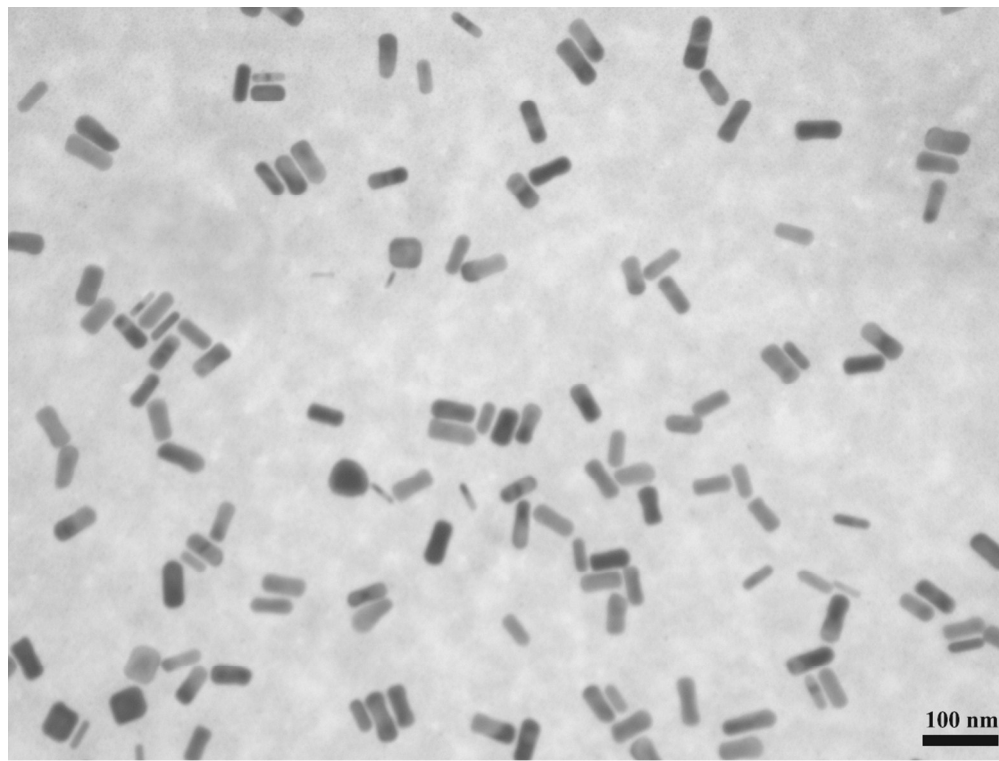


Figure 5a: TEM image of non-centrifuged Au@Ag nanorods in the absence of AFP  
451x339mm (72 x 72 DPI)

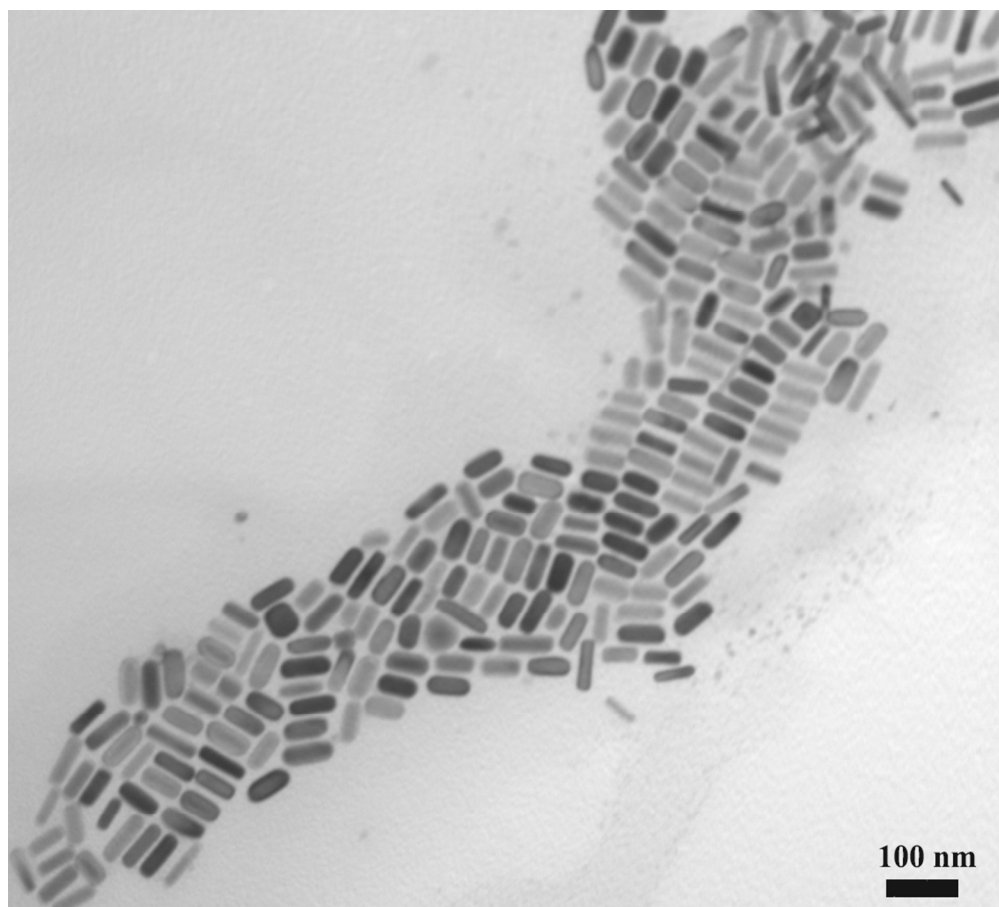


Figure 5b: TEM image of non-centrifuged Au@Ag nanorods in the presence of AFP.  
401x361mm (72 x 72 DPI)

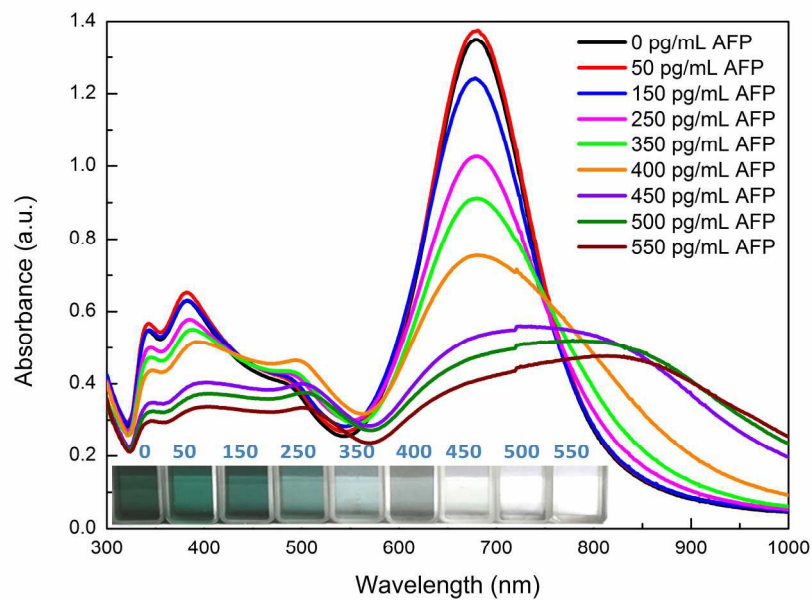


Figure 6a: The absorption spectra of the interaction between centrifuged Au@Ag nanorods and AFP, and the AFP concentration ranges from 0 to 550 pg/mL, the inset: The corresponding color change of centrifuged Au@Ag nanorods upon the addition of AFP with different concentrations ranging from 0 to 550 pg/mL; 209x148mm (300 x 300 DPI)

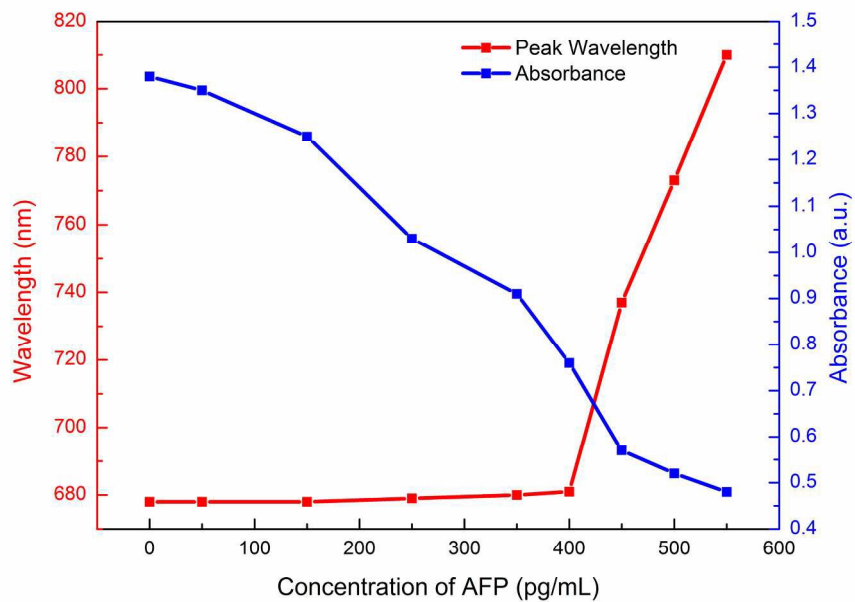


Figure 6b: The AFP concentration-dependent peak wavelength and absorbance change of centrifuged Au@Ag nanorods;  
209x148mm (300 x 300 DPI)

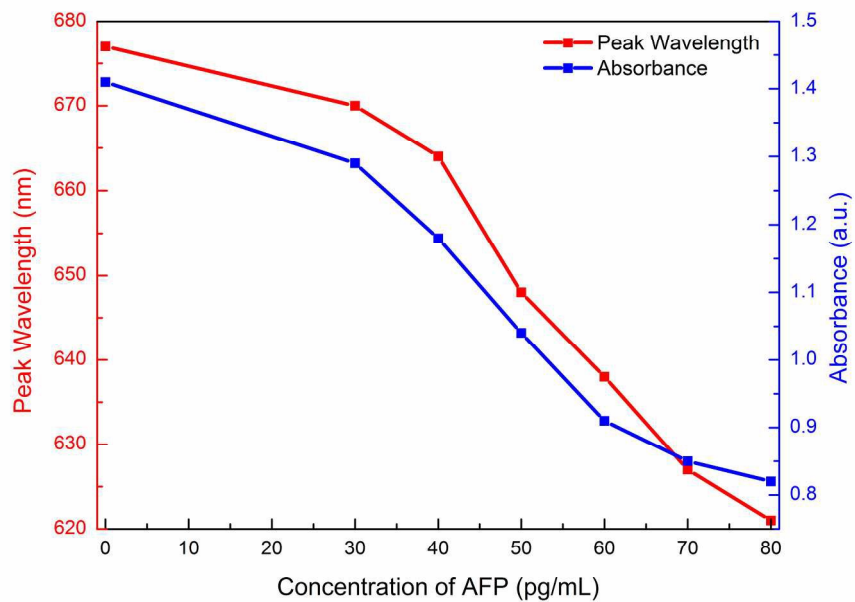


Figure 6c: The AFP concentration-dependent peak wavelength and absorbance change of non-centrifuged Au@Ag nanorods;  
209x148mm (300 x 300 DPI)

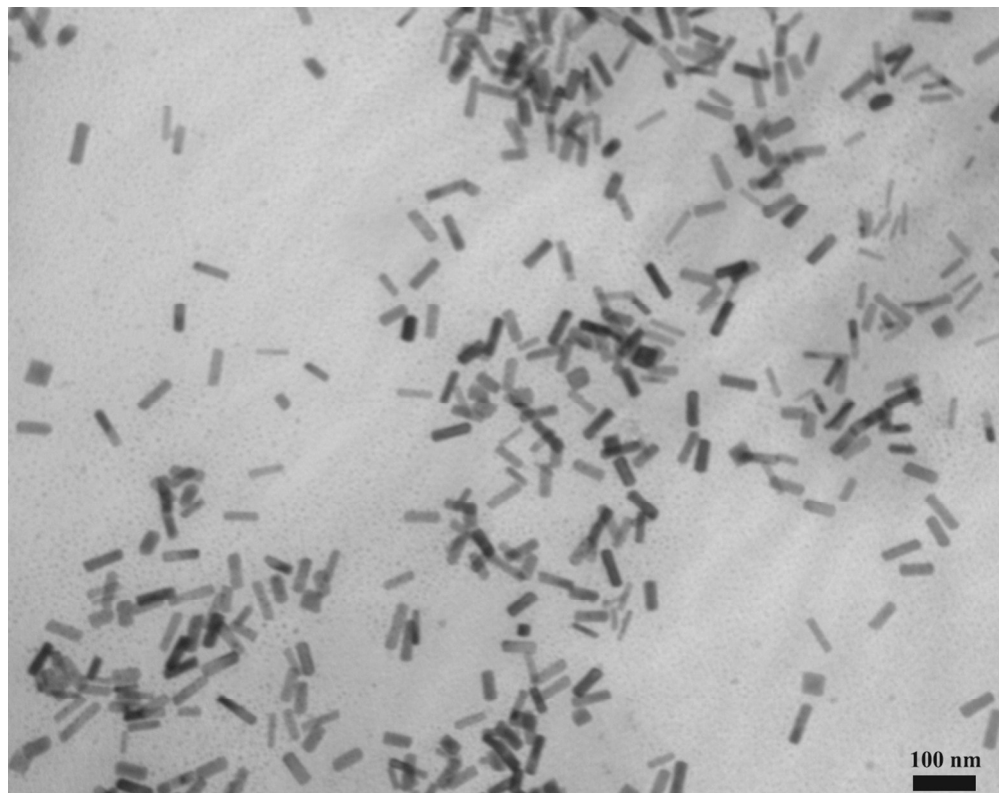


Figure 6d: TEM image of centrifuged Au@Ag nanorods upon the addition of AFP.  
461x365mm (72 x 72 DPI)

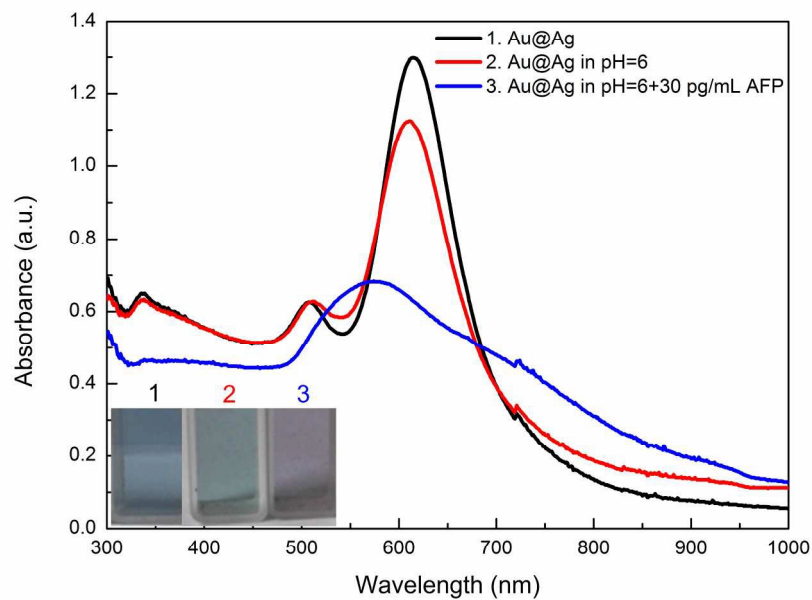


Figure 7a: The absorption spectra change of prepared original Au@Ag nanorods, Au@Ag nanorods in PBS of pH 6 in the absence and presence of AFP, the inset: the corresponding color change of prepared Au@Ag nanorods colloids;  
209x148mm (300 x 300 DPI)

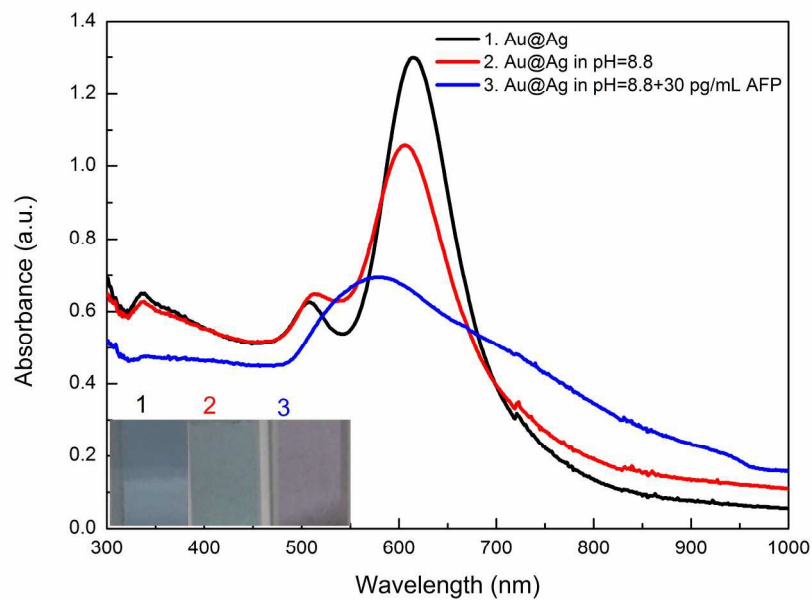


Figure 7b: The absorption spectra change of prepared original Au@Ag nanorods, Au@Ag nanorods in PBS of pH 8.8 in the absence and presence of AFP, the inset: the corresponding color change of prepared Au@Ag nanorods colloids.  
209x148mm (300 x 300 DPI)

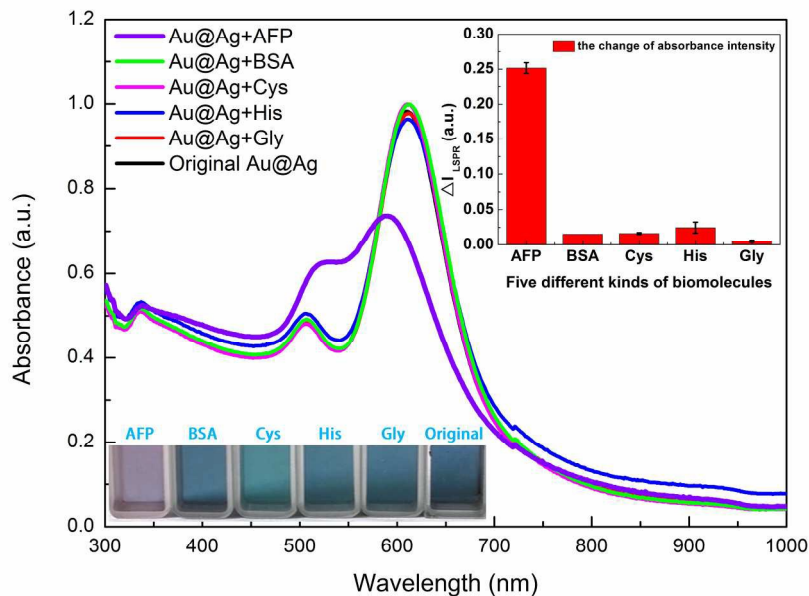


Figure 8: The absorption spectra of Au@Ag nanorods upon the addition of different kinds of biomolecules including AFP, BSA, Cys, His and Gly. The concentration of AFP is 30  $\mu\text{g}/\text{mL}$ , while the concentration of other biomolecules is 30  $\text{ng}/\text{mL}$ , the inset 1: The corresponding color of Au@Ag nanorods upon the addition of AFP, BSA, Cys, His and Gly, the inset 2: The absorbance intensity change of Au@Ag nanorods upon the addition of AFP, BSA, Cys, His and Gly.  
209x148mm (300 x 300 DPI)